ADVANCED MATERIALS

DOI: 10.1002/adma.200800628

Controllable Microfluidic Production of Microbubbles in Water-in-Oil Emulsions and the Formation of Porous Microparticles**

By *Jiandi Wan, Alexander Bick, Matthew Sullivan,* and *Howard A. Stone**

We report the formation of micrometer-diameter water droplets, in a continuous oil phase, where each droplet encapsulates a discrete number of gas bubbles. The approach combines two different microfluidic geometries: flow-focusing and a T-junction (Fig. 1). In particular, monodisperse microbubbles were first generated in a continuous water phase using a flow-focusing geometry, after which the gas-water system was dispersed into a continuous oil phase either by a flow-focusing or a T-junction element so as to obtain water drops that contain individual gas bubbles. The generation of water-encapsulated microbubbles in both geometries is dependent on the flow rates of the two liquids, and it is less sensitive to the gas pressure in the double flow-focusing geometry (DFF; Fig. 1c and d) than in the geometry with flow-focusing followed by a T-junction (FFT; Fig. 1a and b). Moreover, the DFF was able to form a relatively thin water layer encapsulating individual microbubbles while the FFT, on the other hand, had the advantage of controlling of the *number* of bubbles per water droplet. We illustrated this characteristic feature of FFT using an aqueous photopolymerizable acrylamide solution and fabricated monodisperse porous polyacrylamide particles with relatively low elastic moduli compared with solid polyacrylamide particles. These ideas provide an avenue for systematically controlling gas-liquid microstructures of double-emulsion type and offer a new fabrication method for polymer-covered microbubbles and porous microparticles.

Micrometer-dimension bubbles have numerous biomedical applications such as ultrasound contrast agents,[1,2] targeted drug delivery vehicles,[3,4] and can also act as tumor/thrombus-destruction materials.[5–7] Bubbles are also the basic elements for making a wide variety of foamed porous materials, which find many applications from pharmaceuticals to foods and the cosmetic industry. For example, porous particles offer distinct routes for drug delivery[8] and controlled release of chemicals.

There are a wide variety of approaches that have been studied recently for generating two-phase materials, such as monodisperse gas bubbles or droplets made in microchannels and suspended in a continuous fluid phase.[9–12] The drops themselves can be viewed as building blocks for emulsions, can act as isolated containers for chemical reactions, phase behavior and protein crystallization,[13,14] or may be elements in proposed logic devices.[15] These microfluidic methods give control of size and composition on a drop-by-drop basis, generally yield results with low polydispersity, and have been extended to make polymeric particles of various shapes.[16–19] The majority of work to date has focused on two-phase systems.[20]

Here we are interested in the controlled formation of three-phase materials using microfluidic tools to obtain micrometer-dimension structuring. Such double or multiple emulsions are most commonly made using bulk processing techniques.[21] Simple capsules are another example of a three-phase material (liquid, shell, liquid) made from liquid precursors. To achieve drop-by-drop control individual microfluidic devices are usually considered. Recently at least two microfluidic approaches have been used to make double emulsions of two distinct liquids, where control over the size, composition, and number of encapsulated drops in each mother drop was demonstrated.[22–27] The detailed control of the microstructure enabled novel routes for controlled release.[24] We are interested in extending the range of materials to include monodisperse gas-liquid multiple emulsions. An early study of this type demonstrated the generation of millimeter-dimension oil-encapsulated bubbles in a water-continuous phase using a double-tube nozzle technique.[28–30] Here we introduce a method for making gas-liquid-liquid emulsions, with control of the size and number of the encapsulated phase. Finally, we report the further step of polymerization of the compound drops to form monodisperse porous particles. Taken together, these approaches make possible discrete monodisperse microparticles with controlled porosity.

In our microfluidic approaches, we first consider the device with flow focusing followed by a T-junction, or FFT, which allows the controlled formation of multiple micrometer-size bubbles per droplet with the coefficient of variation less than 0.01(see Supporting Information, Fig. S1). In particular, we report in Figure 2 that the number of encapsulated bubbles, all of the same size, in each water droplet is controlled by the flow rate ratio of water to oil (Q_w/Q_o) at constant gas pressure. We have found that we can identify conditions that reproducibly give discrete numbers of gas bubbles per droplet. For example, we have made systems that give one, two, three, four (Fig. 2a–d)

[*] Prof. H. A. Stone, Dr. J. Wan, A. Bick, Dr. M. Sullivan
School of Engineering and Applied Sciences, Harvard University
Cambridge, MA 02138 (USA)
E-mail: has@seas.harvard.edu; jiandi@seas.harvard.edu

[**] The authors would like to thank the Harvard Center for Nanoscale Systems and NSF via the Harvard NSEC for support of this work. Also, the authors thank Sarah Koester, William D. Ristenpart, Amy Rowat, and Anderson Shum for helpful discussions. Supporting Information is available online from Wiley InterScience or from the authors.

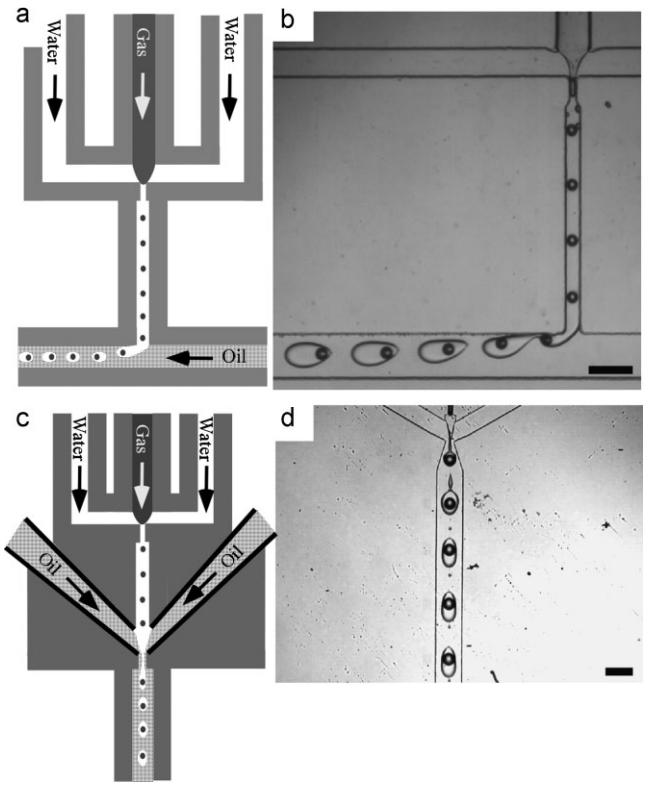

Figure 1. Experimental setups used to generate gas-in-water-in-oil emulsions. a) Illustration and b) experimental image of water droplet encapsulating microbubbles in a flow-focusing then T-junction microfluidic device (FFT). Scale bar: 200 μm. c) Illustration and d) experimental image of water droplet encapsulating microbubbles in a double flow-focusing microfluidic device (DFF). Scale bar: 150 μm. There is 2% (w/w) SDS in the water phase for all experiments.

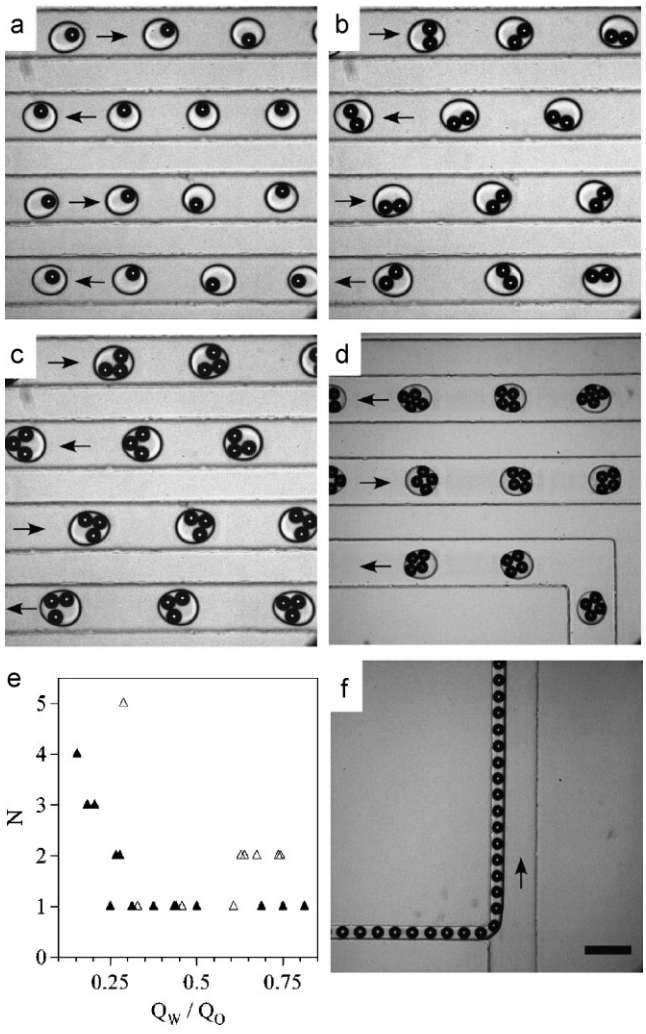

Figure 2. Controlling the number of bubbles in a single water droplet for flow-focusing followed by a T-junction (FFT): a) one bubble per droplet ($Q_w/Q_o = 0.27$), b) two bubbles per droplet ($Q_w/Q_o = 0.28$), c) three bubbles per droplet ($Q_w/Q_o = 0.20$), d) four bubbles per droplet ($Q_w/Q_o = 0.15$). Pressure of the gas phase was constant at 18 psi. e) Number of encapsulated microbubbles (N) as a function of the flow rate ratio of water to oil (Q_w/Q_o) at two different gas pressures. ▲: 18 psi. Δ: 20 psi. f) Train of gas bubbles in a continuous stream of the water phase ($Q_w/Q_o = 1.6$). The dark spheres are gas bubbles and the continuous phase is mineral oil. The small dark arrows indicate the flow direction in each channel. Scale bar: 200 μm.

or even more bubbles per droplet. The gas bubbles do not coalesce. In addition, in general we have noticed that the gas bubbles tend to be organized near the front of the drop (the small dark arrows indicate the flow direction in each channel), which is consistent with the flow inside the drop and the fact that the bubbles are sufficiently large that they cannot simply recirculate as would a small tracer particle. Furthermore, by adjusting the gas pressure, as shown in Figure 2e we observed regimes where the number of encapsulated bubbles is either independent of the gas pressure ($Q_w/Q_o = 0.3$–0.6) or dependent on the gas pressure ($Q_w/Q_o = 0.6$–$0.9; 0.25$–0.3). If the flow rate ratio of water to oil is lower than 0.15 or higher than 1, it is beyond the regime where gas-in-water-in-oil emulsions can form steadily and gives either a string of gas bubbles in a continuous water phase (Fig. 2f) or water droplets with no bubbles at all.

We then focused on the effect of the flow rates and gas pressure on the formation of the 'single bubble per drop' regime in both FFT and DFF devices. In Figure 3a and c, we plotted the drop and bubble diameter (d) relative to the orifice width (D) at different gas pressures as a function of the flow rate ratio of water to oil (Q_w/Q_o) in FFT and DFF respectively. We noticed that, once the gas-in-water-in-oil emulsions were formed in both devices, the sizes of the encapsulated bubbles were strongly dependent on the relative flow rate (Q_w/Q_o), but the sizes of mother droplets did not depend significantly on Q_w/Q_o. This feature allows control of the thickness of the water layer. We also observed that the gas pressure played a minor role in the DFF device, but it significantly affected the droplet size in the FFT device, which is consistent with the reported role of the gas pressure in the break-up mechanism in a typical T-junction geometry.[31] By plotting the scaled bubble diameter (d_{bubble}) relative to the drop diameter (d_{drop}) as a

ADVANCED MATERIALS

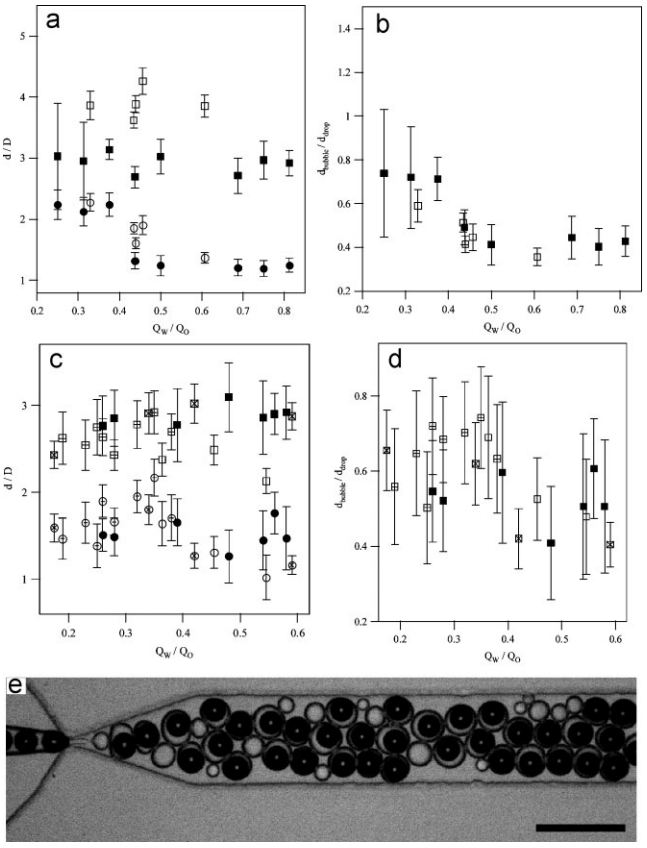

Figure 3. Effect of the flow rate ratio of water to oil (Q_w/Q_o) on the size of water droplets and encapsulated bubbles (where there is only one bubble per droplet) in (a, b) flow-focusing followed by a T-junction (FFT) and (c, d) double flow-focusing device (DFF). a) Scaled drop (d_{drop}) and bubble (d_{bubble}) diameter relative to the orifice width (D) as a function of Q_w/Q_o in FFT. ■: droplet at 18 psi. ●: bubble at 18 psi. □: droplet at 20 psi. ○: bubble at 20 psi. b) Scaled bubble diameter (d_{bubble}) relative to the drop diameter (d_{drop}) as a function of Q_w/Q_o in FFT. ■: 18 psi. □: 20 psi. c) Scaled drop and bubble diameter (d) relative to the orifice width (D) as a function of Q_w/Q_o in DFF. □: droplet at 13 psi. ○: bubble at 13 psi. ■: droplet at 18 psi. ●: bubble at 18 psi. ⊞: droplet at 19 psi. ⊕: bubble at 19 psi. ⊠: droplet at 20 psi. ⊗: bubble at 20 psi. d) Scaled bubble diameter (d_{bubble}) relative to drop diameter (d_{drop}) as a function of Q_w/Q_o in DFF. □: 13 psi. ■: 18 psi. ⊞: 19 psi. ⊠: 20 psi. e) Image of the formation of thin water layers (~5 μm) that encapsulate microbubble emulsions ($Q_w/Q_o = 1$; 14 psi) in DFF. The dark spheres are gas bubbles and the continuous phase is mineral oil. Scale bar: 150 μm.

function of Q_w/Q_o in both FFT and DFT devices (Fig. 3b and d), we observed a dependence of the thickness of the water layer on the relative flow rate in both devices. In particular, for the DFF device, when $Q_w/Q_o = 0.35$ we obtained 90 μm diameter gas bubbles surrounded by 17 μm thick water layers (see Supporting Information, Fig. S2). Changing the relative flow rate to unity, we measured water layers with thickness as small as 5 μm and encapsulated bubbles with diameter around 20 μm, as shown in Figure 3e. This control of the thickness of an aqueous layer provides a microfluidic route for the fabrication of microbubbles covered with thin layers of polymer, as has been demonstrated for the analogous three-liquid phase system.[24]

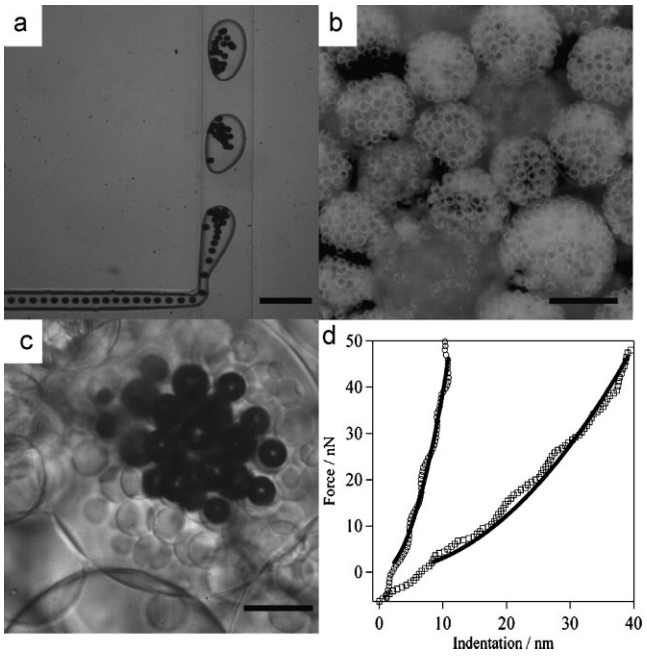

Figure 4. Generation of porous polyacrylamide microparticles and their elastic properties. a) Image of sequential formation of multiple bubbles per drop in a flow-focusing followed by a T-junction device (FFT) ($Q_w/Q_o = 1$; $P = 18$ psi). Scale bar 200 μm. b) Inverted image of collected drops with encapsulated microbubbles. Scale bar 200 μm. c) Image of an acrylamide droplet with bubbles after UV irradiation. Scale bar 50 μm. d) Force indentation curves of dry polyacrylamide particles when photopolymerized with (□, lower curve) and without bubbles (○, upper curve). The black solid lines represent the fit by the tip model (Eq. 1) to the indentation data on the polyacrylamide particles when photopolymerized with bubbles (lower curve, open square, $E = (3.6 \pm 1.2) \times 10^7$ Pa) and without bubbles (upper curve, open circles, $E_s = (8.6 \pm 1.7) \times 10^8$ Pa).

We have also identified flow conditions in the FFT where we get a large number of gas bubbles in each water droplet. We thus were able to fabricate porous particles by first making droplets containing many gas bubbles and then polymerizing the aqueous phase. Figure 4a and b, respectively, show the sequential generation of photopolymerizable acrylamide aqueous droplets with encapsulated microbubbles ($Q_w/Q_o = 1$) and the collection of these droplets in the reservoir before UV irradiation. Figure 4c shows a magnified view of one acrylamide aqueous droplet after UV irradiation and many trapped bubbles are evident. The objects are effectively microspheres of a closed-cell foam. Once the bubbles were trapped inside water droplets or the polymerized polyacrylamide particles, they were stable for as long as 60 minutes before significant dissolution was evident (see Supporting Information, Fig. S3).

The effective elastic modulus of the dry photopolymerized polyacrylamide particles with and without entrapped microbubbles was investigated using atomic force microscope (AFM) (Fig. 4d). The porous polyacrylamide particles show relatively low elastic moduli ($E = (3.6 \pm 1.2) \times 10^7$ Pa) compared to the particles without bubbles ($E_s = (8.6 \pm 1.7) \times 10^8$ Pa). We note that $E/E_s = 0.04$. An estimate of the gas fraction obtained by approximating the number of gas bubbles

in the porous particles gives an effective density of $0.27\rho_s$, where ρ_s is the density of the polymerized polyacrylamide. These results are consistent with macroscopic measurements of the elasticity of other closed-cell foams.[32] Thus, our ability to tune the number of gas bubbles per droplet offers an approach to manipulate the elasticity of individual microparticles by changing the internal porosity.

In summary, we have reported a microfluidic approach with two different geometries to generate gas-in-water-in-oil (three-phase) emulsions and systemically investigated the effects of the liquid flow rates and that gas pressure on the formation of water-encapsulated microbubbles. By changing the microfluidic geometry and relative flow rate, we achieved both control over the thickness of the water layer to obtain thin shells covering individual microbubbles and we have demonstrated control over the number of encapsulated bubbles. Adding photopolymerizable monomers (acrylamide) into the aqueous phase, we obtained porous polyacrylamide particles with relatively low elastic moduli compared to the solid polyacrylamide particles. This technology has the potential to generate thin-polymer covered microbubbles or porous biopolymer microparticles for applications in ultrasound contrast materials, tissue engineering materials, micro-reactors and other areas where porous microstructures are advantageous or required.

Experimental

Fabrication of Microfluidic Devices and Experimental Setup: Microfluidic chips were fabricated in PDMS using standard soft photolithography techniques [33]. The water and oil are loaded in two syringes (Hamilton) respectively and connected to syringe pumps (Kd Scientific, KDS101). Pressure is applied to the needle independently controlled by a regulator (Bellofram, St. Louis, MO) with a precision of 0.1 psi. Polyethylene (PE 20) tubes are connected from the syringe needle to the inlet hole of the channel of the device. Before use, the microfluidic chips were treated with octadecyltrichlorosilane (OTS) to make the glass surface hydrophobic.

The illustrations of the double flow-focusing (DFF) and flow-focusing followed by a T-junction (FFT) microfluidic devices are shown in Figure 1. The height of the channels is everywhere equal 38 μm as measured with surface profilometer. The widths of the gas and water channels are 100 μm; the width of the central channel where gas bubbles were dispersed in the water phase is 60 μm; the width of the oil channel is 150 μm (DFF) or 200 μm (FFT); and the widths of the orifices for all geometries are either 20 or 30 μm. For the flow-rate dependent measurements, we dispersed pure nitrogen gas bubbles into deionized water with sodium dodecyl sulfate (SDS) (2 wt %, Aldrich) after which the water droplets with bubble(s) were dispersed into the mineral oil (Aldrich).

For the photopolymerization reactions [34], acrylamide (36 wt %, Aldrich), *N*,*N*-methylenebisacrylamide (1.5 wt %, Aldrich) and 2,2-diethoxyacetophenone (0.5 wt %, Aldrich) were dissolved in the water phase (deionized water) and 2,2-diethoxyacetophenone (5 wt %) was dissolved in the oil phase (PDMS fluid 200 and 749, Dow Corning). The acrylamide droplets were polymerized by activating the photoinitiator using a 100 W mercury lamp coupled into a 10 × microscope lens (NA = 0.25) on an inverted fluorescence microscope (Leica, Bannockburn, IL).

Microbubble emulsions are directly observed using a high-speed video camera (Phantom V 9, 1400 frames per second) mounted on the microscope. The size distributions of the droplets and encapsulated bubbles are analyzed using an image analysis program written in-house with Matlab software.

Atomic Force Microscope Measurement: Elastic properties of the dry polyacrylamide particles were characterized by indentation measurements on a MFP-3D Coax atomic force microscope (AFM) coupled with an invert microscope (Asylum Research, Santa Barbara, CA). A silicon nitride probe (MikroMash, OR) with a force constant of $\sim 0.15\,\mathrm{N\,m^{-1}}$ was applied in the force mode. After the measurement, the collected force curves were converted into force versus indentation graphs using software provided by Asylum Research. The elastic moduli of the particles were determined by assuming a conical tip shape, which produces a load-indentation dependence [19]

$$F = \frac{2E\tan\alpha}{\pi(1-\upsilon^2)}\delta^2 \quad (1)$$

where F is the loading force (N), δ is the indentation (m), E is Young's modulus (Pa), υ is the Poisson's ratio (0.5), and α is the tip semivertical angle (35°).

Received: March 11, 2008
Revised: April 28, 2008
Published online: July 14, 2008

[1] J. R. Lindner, *Nat. Rev. Drug Discovery* **2004**, *3*, 527.
[2] E. G. Schutt, D. H. Klein, R. M. Mattrey, J. G. Riess, *Angew. Chem. Int. Ed.* **2003**, *42*, 3218.
[3] K. Ferrara, R. Pollard, M. Borden, *Annu. Rev. Biomed. Eng.* **2007**, *9*, 415.
[4] Y. Liu, H. Miyoshi, M. Nakamura, *J. Controlled Release* **2006**, *114*, 89.
[5] H. Leong-Poi, J. Christiansen, A. L. Klibanov, S. Kaul, J. R. Lindner, *Circulation* **2003**, *107*, 455.
[6] C. A. Molina, M. Ribo, M. Rubiera, J. Montaner, E. Santamarina, R. Delgado-Mederos, J. F. Arenillas, R. Huertas, F. Purroy, P. Delgado, J. Alvarez-Sabin, *Stroke* **2006**, *37*, 425.
[7] E. C. Unger, T. Porter, W. Culp, R. Labell, T. Matsunaga, R. Zutshi, *Adv. Drug Delivery Rev.* **2004**, *56*, 1291.
[8] D. A. Edwards, A. Ben-Jebria, R. Langer, *J. Appl. Physiol.* **1998**, *84*, 379.
[9] S. L. Anna, N. Bontoux, H. A. Stone, *Appl. Phys. Lett.* **2003**, *82*, 364.
[10] V. Barbier, M. Tatoulian, H. Li, F. Arefi-Khonsari, A. Ajdari, P. Tabeling, *Langmuir* **2006**, *22*, 5230.
[11] P. Garstecki, I. Gitlin, W. DiLuzio, G. M. Whitesides, E. Kumacheva, H. A. Stone, *Appl. Phys. Lett.* **2004**, *85*, 2649.
[12] M. Seo, C. Paquet, Z. Nie, S. Xu, E. Kumacheva, *Soft Matter* **2007**, *3*, 986.
[13] J-u. Shim, G. Cristobal, D. R. Link, T. Thorsen, Y. Jia, K. Piattelli, S. Fraden, *J. Am. Chem. Soc.* **2007**, *129*, 8825.
[14] B. Zheng, C. J. Gerdts, R. F. Ismagilov, *Curr. Opin. Struct. Biol.* **2005**, *15*, 548.
[15] M. Prakash, N. Gershenfeld, *Science* **2007**, *315*, 832.
[16] D. Dendukurl, D. C. Pregibon, J. Collins, T. A. Hatton, P. S. Doyle, *Nat. Mater.* **2006**, *5*, 365.
[17] Z. Nie, W. Li, M. Seo, S. Xu, E. Kumacheva, *J. Am. Chem. Soc.* **2006**, *128*, 9408.
[18] Z. Nie, S. Xu, M. Seo, P. C. Lewis, E. Kumacheva, *J. Am. Chem. Soc.* **2005**, *127*, 8058.
[19] H. Zhang, E. Tumarkin, R. Peerani, Z. Nie, R. M. A. Sullan, G. C. Walker, E. Kumacheva, *J. Am. Chem. Soc.* **2006**, *128*, 12205.
[20] A. Günther, K. F. Jensen, *Lab Chip* **2006**, *6*, 1487.

ADVANCED MATERIALS

[21] J. Bibette, F. Leal-Calderon, V. Schmitt, P. Poulin, *Emulsion Science*, Springer, Berlin **2003**.
[22] L.-Y. Chu, A. S. Utada, R. K. Shah, J.-W. Kim, D. A. Weitz, *Angew. Chem. Int. Ed.* **2007**, *46*, 8970.
[23] T. Nisisako, S. Okushima, T. Torii, *Soft Matter* **2005**, *1*, 23.
[24] A. S. Utada, E. Lorenceau, D. R. Link, P. D. Kaplan, H. A. Stone, D. A. Weitz, *Science* **2005**, *308*, 537.
[25] J.-W. Kim, A. S. Utada, A. Fernandez-Nieves, N. Hu, Z. Hu, D. A. Weitz, *Angew. Chem. Int. Ed.* **2007**, *46*, 1819.
[26] E. Lorenceau, A. S. Utada, D. R. Link, G. Cristobal, M. Joanicot, D. A. Weitz, *Langmuir* **2005**, *21*, 9183.
[27] S.-H. Kim, S.-J. Jeon, S.-M. Yang, *J. Am. Chem. Soc.* **2008**, *130*, 6040.
[28] T. Hayakawa, M. Shigeta, *J. Chem. Eng. Jpn.* **1973**, *6*, 273.
[29] T. Hayakawa, M. Shigeta, *J. Chem. Eng. Jpn.* **1974**, *7*, 140.
[30] Y. H. Mori, Y. Kogo, K. Kaminaga, *J. Chem. Technol. Biotechnol.* **1989**, *45*, 311.
[31] P. Garstecki, M. J. Fuerstman, H. A. Stone, G. M. Whitesides, *Lab Chip* **2006**, *6*, 437.
[32] L. J. Gibson, M. F. Ashby, *Cellular Solids: Structure and Properties*, Pergamon Press, Oxford **1988**.
[33] D. C. Duffy, J. C. McDonald, O. J. A. Schueller, G. M. Whitesides, *Anal. Chem.* **1998**, *70*, 4974.
[34] R. F. Shepherd, J. C. Conrad, S. K. Rhodes, D. R. Link, M. Marquez, D. A. Weitz, J. A. Lewis, *Langmuir* **2006**, *22*, 8618.